

Modulation of intersubband infrared absorption under intense terahertz irradiation

A. Hernández-Cabrera* and P. Aceituno

Dpto. Física Básica, Universidad de La Laguna, La Laguna, 38206-Tenerife, Spain

F. T. Vasko

Institute of Semiconductor Physics, NAS Ukraine, Prospekt Nauki 41, Kiev, 03028, Ukraine

(Received 5 April 2005; published 6 July 2005)

We analyze the modification of the intersubband absorption of electrons in quantum wells under intense THz irradiation. An expression for the induced current is obtained, based on the adiabatic approach and the resonant approximation. We predict the occurrence of a significant fine structure as well as the broadening and shift of the absorption under THz pump in a MW cm⁻² intensity range.

DOI: [10.1103/PhysRevB.72.045307](https://doi.org/10.1103/PhysRevB.72.045307)

PACS number(s): 73.63.Hs, 78.45.+h, 78.47.+p

I. INTRODUCTION

Strong transverse fields have long been known for modifying confined states in quantum wells (QWs). The examination of the interband optical transitions under transverse fields, both static and high-frequency, is a convenient method to study these modifications (see references in Refs. 1–3 and Refs. 4 and 5, respectively). The excitonic effect and the modifications of both electron and hole states under transverse fields have to be taken into account for a quantitative description of the interband linear response. It is also interesting to study the intersubband response under infrared (IR) excitation of electrons between the ground and the excited conduction band states which are placed in a transverse field. Whereas the electro-optic modulation of the intersubband transitions is well investigated,⁶ the influence of an intense THz irradiation on such transitions is not investigated to the best of our knowledge. In this paper we treat theoretically the effect of the THz pump on the infrared (IR) intersubband absorption.

The confined electron states in a QW, of width d , subjected to a transverse electric field $E_\omega \cos \omega t$, are described within the adiabatic approach, if $\hbar\omega \ll \varepsilon_{21}$, where ε_{21}/\hbar is the frequency of the intersubband transitions. Since the levels oscillate with a frequency ω , the $(n+1)$ -order intersubband transitions, with n THz photons and a single IR photon, take place resulting in a fine structure of the absorption. At the same time, the shape of the absorption peaks is modified under the THz irradiation. In addition, one may consider the THz irradiation as a perturbation if $|e|E_\omega d/2 < \varepsilon_{21}$. Otherwise, a numerical description of the electron states has to be applied.

The calculations below are based on the one-particle density matrix equation linearized with respect to the IR field $E_\Omega \exp(-i\Omega t)$, while the THz irradiation is taken into account in the framework of the adiabatic approach. The broadening is described by the phenomenological approach which takes into account the LO-phonon emission in the spectral region $\Omega > \omega_{LO}$, where ω_{LO} is the optical phonon frequency. We have considered two cases: a symmetric rectangular QW and a nonsymmetric one. The last case may be realized by adding a transversal dc electric field E_o to the symmetric

case, as can be seen in Fig. 1(a) and 1(b), respectively.

The paper is organized as follows. In Sec. II we derive the relative intersubband absorption under THz pump starting on the density matrix equation. The case of the perturbative approach is considered in Sec. III, while the results for the numerical description are discussed in Sec. IV. Concluding remarks and a list of assumptions made are given in the last section.

II. INTERSUBBAND RESPONSE

In this section, we obtain the averaged over the THz pump period relative absorption of the IR probe. The high-frequency addendum to the density matrix $\Delta\rho_{\mathbf{r}}(z, z') \exp(-i\Omega t)$ is governed by the linearized equation written in the coordinate-momentum representation:

$$\begin{aligned} \frac{\partial \Delta\rho_{\mathbf{r}}(z, z')}{\partial t} &+ \frac{i}{\hbar} (\hat{h}_{z\mathbf{r}} - \hat{h}_{z'\mathbf{r}} - \hbar\Omega) \Delta\rho_{\mathbf{r}}(z, z') + \frac{i}{\hbar} (\delta\hat{h}_z - \delta\hat{h}_{z'}) \rho_{\mathbf{r}}(z, z') \\ &= 0 \end{aligned} \quad (1)$$

with the transverse coordinate z and 2D momentum \mathbf{p} . Here

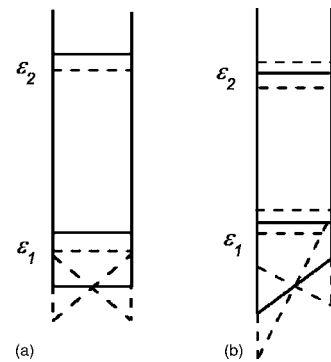


FIG. 1. The band diagrams for symmetric (a) and nonsymmetric (b) QWs under transverse THz irradiation. Dashed lines schematically show variation of levels and potentials under maximal THz field.

the Hamiltonian and the perturbation operator, $\hat{h}_{z,t}$ and $\delta\hat{h}_z \exp(-i\Omega t)$, are given by

$$\hat{h}_{z,t} = \frac{\hat{p}_z^2}{2m} + w_z + eE_{\omega z} \cos \omega t, \quad \delta\hat{h}_z = \frac{ie}{\Omega} E_{\Omega} \hat{v}_z, \quad (2)$$

where $\hat{v}_z = \hat{p}_z/m$ is the velocity operator and w_z is the potential energy inside the QW. Within the hard-wall approximation one has to consider the interval $|z| < d/2$ with the zero boundary conditions. The density matrix under THz irradiation satisfies the periodicity condition: $\rho_{\mathbf{p}t+2\pi/\omega}(z, z') = \rho_{\mathbf{p}t}(z, z')$.

It is convenient to use the parametrically time-dependent wave functions, $\varphi_{z,t}^k$, determined by the eigenstate problem:

$$\hat{h}_{z,t} \varphi_{z,t}^k = \varepsilon_{kt} \varphi_{z,t}^k, \quad \varphi_{z=\pm d/2,t}^k = 0, \quad (3)$$

which is defined in the interval $|z| < d/2$. The expansion of the first- and zeroth-order density matrices $\Delta\rho_{\mathbf{p}t}(z, z')$ and $\rho_{\mathbf{p}t}(z, z')$ over this basis gives us

$$\begin{aligned} \Delta\rho_{\mathbf{p}t}(z, z') &= \sum_{kk'} \Delta\rho_{\mathbf{p}t}(k, k') \varphi_{z,t}^{k*} \varphi_{z',t}^{k'}, \\ \rho_{\mathbf{p}t}(z, z') &= \sum_{kk'} \rho_{\mathbf{p}t}(k, k') \varphi_{z,t}^{k*} \varphi_{z',t}^{k'}, \end{aligned} \quad (4)$$

and Eq. (1) in the k -representation takes the form

$$\begin{aligned} \frac{\partial \Delta\rho_{\mathbf{p}t}(k, k')}{\partial t} + \frac{i}{\hbar} (\varepsilon_{kt} - \varepsilon_{k't} - \hbar\Omega) \Delta\rho_{\mathbf{p}t}(k, k') \\ + \sum_{k'} [\Delta\rho_{\mathbf{p}t}(k, k') \delta_t^{k'k} - \delta_t^{kk'} \Delta\rho_{\mathbf{p}t}(k', k)] \\ = \frac{i}{\hbar} \sum_{k'} [\delta h_t^{kk'} \rho_{\mathbf{p}t}(k', k) - \rho_{\mathbf{p}t}(k, k') \delta h_t^{k'k}]. \end{aligned} \quad (5)$$

Here, the nonadiabatic factor $\delta_t^{kk'}$ appears because we have used the parametrically time-dependent basis determined by Eq. (3). This factor and the perturbation $\delta h_t^{kk'}$ are given by the standard expressions:

$$\begin{aligned} \delta_t^{kk'} &= \int_{-d/2}^{d/2} dz \frac{\partial \varphi_{z,t}^{k*}}{\partial t} \varphi_{z,t}^{k'}, \\ \delta h_t^{kk'} &= \frac{ie}{\Omega} E_{\Omega} \int_{-d/2}^{d/2} dz \varphi_{z,t}^{k*} \hat{v}_z \varphi_{z,t}^{k'}. \end{aligned} \quad (6)$$

We have taken into account that $\delta_t^{k'k} = -\delta_t^{kk'}$.

The induced current density is written through $\Delta\rho$ as follows:

$$\begin{aligned} j_t &= \frac{e}{L^2} \sum_{\mathbf{p}} \int_{-d/2}^{d/2} dz \lim_{z_1, z'_1 \rightarrow z} (\hat{v}_{z_1} + \hat{v}_{z'_1}) \Delta\rho_{\mathbf{p}t}(z_1, z'_1) \\ &= \frac{2e}{L^2} \sum_{\mathbf{p}kk'} v_{k'k}(t) \Delta\rho_{\mathbf{p}t}(k, k'), \end{aligned} \quad (7)$$

where L^2 is the normalization area and $v_{kk'}(t)$

$= \int_{-d/2}^{d/2} dz \varphi_{z,t}^{k*} \hat{v}_z \varphi_{z,t}^{k'}$. For the case of resonant excitation between first and second levels, when $\hbar\Omega \sim \varepsilon_{21}$, Eq. (7) can be transformed into $j_t \approx ev_{12}(t) \Delta\rho_t(2, 1)$. Here we have also performed the summation over 2D momentum according to $\Delta\rho_t(2, 1) = (2/L^2) \sum_{\mathbf{p}} \Delta\rho_{\mathbf{p}t}(2, 1)$. Using Eq. (5) and supposing that only the ground level is populated, we obtain an equation for $\Delta\rho_t(2, 1)$ in the form

$$\frac{\partial \Delta\rho_t(2, 1)}{\partial t} + i[\Omega_{21}(t) - \Omega - iv_{\Omega}] \Delta\rho_t(2, 1) = \frac{eE_{\Omega}}{\hbar\Omega} v_{21}(t) n_{2D}, \quad (8)$$

where $\Omega_{21}(t) = (\varepsilon_{2t} - \varepsilon_{1t})/\hbar$ is the time-dependent interlevel frequency and n_{2D} is the electron concentration. The stepped effective relaxation-frequency ν_{Ω} increases in the active region, $\Omega > \omega_{LO}$, due to emission of LO-phonons with the frequency ω_{LO} . We have also taken into account that $\delta_t^{kk} = 0$. Therefore, the nonadiabatic factors vanish under the resonant approximation used.

Introducing the time-dependent conductivity tensor $\sigma_{\Omega t} = j_t/E_{\Omega}$ and solving Eq. (8), we write

$$\begin{aligned} \sigma_{\Omega t} &= \frac{e^2 n_{2D}}{\hbar\Omega} v_{21}(t) \int_{-\infty}^t dt' v_{21}(t') \\ &\times \exp\left(-i \int_{t'}^t d\tau [\Omega_{21}(\tau) - \Omega - iv_{\Omega}]\right). \end{aligned} \quad (9)$$

The averaged over the THz period relative absorption is determined as follows:³

$$\xi_{\Omega} = \frac{4\pi}{c\sqrt{\epsilon}} \text{Re} \int_{-\pi/\omega}^{\pi/\omega} \frac{dt}{2\pi/\omega} \sigma_{\Omega t}. \quad (10)$$

Thus, in order to calculate ξ_{Ω} one needs to find $\Omega_{21}(t)$ and $v_{21}(t)$ and to perform the integrations over time.

III. PARABOLIC APPROACH

The perturbative solution of the eigenstate problem (3) can be written as follows:

$$\varphi_{z,t}^k = \varphi_z^k + \sum_{k' \neq k} \frac{eE_{\omega z} z_{kk'}}{\varepsilon_k - \varepsilon_{k'}} \varphi_z^{k'} \cos \omega t + \dots,$$

$$\varepsilon_{kt} \approx \varepsilon_k + eE_{\omega z} z_{kk} \cos \omega t + \sum_{k' \neq k} \frac{|eE_{\omega z} z_{kk'}|^2}{\varepsilon_k - \varepsilon_{k'}} \cos^2 \omega t, \quad (11)$$

where the matrix elements $z_{kk'}$ and the energy level ε_k are determined from the zero-field eigenstate problem: $(\hat{p}_z^2/2m + w_z) \varphi_z^k = \varepsilon_k \varphi_z^k$, with the boundary conditions $\varphi_{|z|=d/2} = 0$. The frequency $\Omega_{21}(t)$ in Eq. (9) is written as follows:

$$\Omega_{21}(t) = \Omega_{21} + \Omega_{21}^{(1)} \cos \omega t + \Omega_{21}^{(2)} \cos 2\omega t, \quad (12)$$

where the coefficients $\Omega_{21}^{(1,2)}$ are obtained from ε_{kt} given by Eq. (11). Note also that $z_{kk} = 0$ for the symmetric QW and the time-dependent contribution to $\Omega_{21}(t)$ is $\propto \cos 2\omega t$ for such a case.

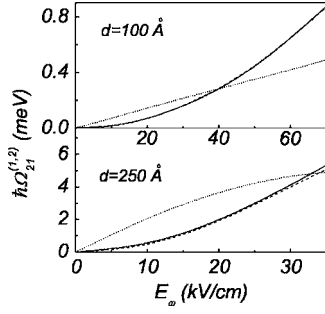


FIG. 2. The coefficients $\hbar\Omega_{21}^{(1,2)}$ versus THz field strength for narrow and wide QWs. Solid line: $\hbar\Omega_{21}^{(2)}$ for symmetric case ($E_0=0$ kV cm $^{-1}$). Dashed (dotted) line: $\hbar\Omega_{21}^{(2)}$ ($\hbar\Omega_{21}^{(1)}$) for nonsymmetric case (QWs under dc field $E_0=10$ kV cm $^{-1}$).

The parabolic and linear dependencies of $\Omega_{21}^{(2)}$ and $\Omega_{21}^{(1)}$ on the applied THz field for both symmetric and asymmetric cases are plotted in Fig. 2. The calculations are performed for narrow ($d=100$ Å) and wide ($d=250$ Å) GaAs-based QWs. In order to model nonsymmetric QW we have introduced a transverse dc field $E_0=10$ kV cm $^{-1}$ besides the THz field $E_\omega \cos \omega t$. We can see in Fig. 2 that the behavior of $\Omega_{21}^{(2)}$ coefficients is exactly the same for the symmetric and nonsymmetric cases in the region where the parabolic approximation is valid ($|e|E_\omega d/2 < \epsilon_{21}$). That is, for the narrow QW a parabolic bearing can be found up to very strong fields ($E_\omega \sim 300$ kV cm $^{-1}$), whereas, for the wide QW, this approximation is only valid up to $E_\omega \sim 20$ kV cm $^{-1}$ and beyond these regions $\Omega_{21}(t)$ cannot be written by means of Eq. (12). For the nonsymmetric case, $\Omega_{21}^{(1)}$ coefficients show an almost linearly increase in the parabolic approximation range for both narrow and wide QWs. After that, $\Omega_{21}^{(1)}$ tend to a constant value.

The velocity matrix element modifies weakly with time, $v_{21}(t) \approx v_{21}$, because the time-dependent contributions ($\propto \cos \omega t, \cos 2\omega t$) are two orders smaller than v_{21} . We have neglected these contributions below. For the structures under consideration $v_{21} \approx 4 \times 10^7$ cm s $^{-1}$ ($d=100$ Å) and $v_{21} \approx 2 \times 10^7$ cm s $^{-1}$ ($d=250$ Å).

Using the expansion of the exponential factors in (9) over the Bessel functions⁷ and performing the integrations over time, we obtain ξ_Ω for the symmetric QW in the form

$$\xi_\Omega \approx \frac{4\pi e^2 \nu_\Omega |v_{21}|^2}{\sqrt{\epsilon} \hbar c \Omega} n_{2D} \sum_{k=-\infty}^{\infty} \frac{J_k(\Omega_{21}^{(2)}/4\omega)^2}{(\Omega_{21} - 2k\omega - \Omega)^2 + \nu_\Omega^2}. \quad (13)$$

In Fig. 3 we have plotted the spectral dependencies of ξ_Ω , given by Eq. (13), under different THz pumps for the narrow

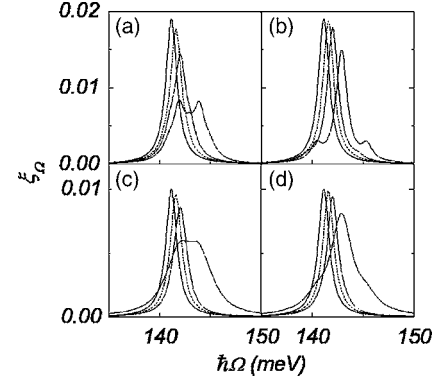


FIG. 3. The spectral dependencies of ξ_Ω versus $\hbar\Omega$ for the symmetric case under THz field strengths: $E_\omega=0$ kV cm $^{-1}$ (solid line), $E_\omega=50$ kV cm $^{-1}$ (dashed line), $E_\omega=70$ kV cm $^{-1}$ (dotted line), and $E_\omega=100$ kV cm $^{-1}$ (dot-dashed line). (a) $\hbar\omega=0.5$ meV, $\hbar\nu=0.66$ meV; (b) $\hbar\omega=1.5$ meV, $\hbar\nu=0.66$ meV; (c) $\hbar\omega=0.5$ meV, $\hbar\nu=1.5$ meV; and (d) $\hbar\omega=1.5$ meV, $\hbar\nu=1.5$ meV.

symmetric QW. The calculations are performed for a multiple quantum well structure with ten decoupled 100 Å wide GaAs QWs and for THz quanta energy values $\hbar\omega=0.5$ and 1.5 meV. We have used two broadening energy values $\hbar\nu \approx 0.66$ meV (corresponding to a relaxation frequency $\nu = 1$ ps $^{-1}$) and $\hbar\nu=1.5$ meV. One can see that, for fields well below the parabolic approximation limit, the relative absorption shows a monotonous decreasing while spreads to higher frequencies. For high fields, beyond 70 kV cm $^{-1}$, a clear multi-peak structure appears because the strong-modulation case, when $\Omega_{21}^{(2)}/4\omega > 1$, can be realized in the framework of the perturbation approach. The relative height of the different peaks for this structure depends on the quanta energy value, as can be seen from Fig. 3, due to the ω contribution to the Bessel functions and the denominators in Eq. (13). Panels (a) and (c), with 0.5 meV, show higher lateral peaks than the central one, whereas panels (b) and (d), with 1.5 meV, have a clear maximum in a central peak. The relaxation energy not only affects the broadening of the peaks but also the relative absorption and, so, panels (c) and (d) with 1.5 meV show wider and lower peaks than panels (a) and (b) in which the fine structure is more evident and the relative absorption is about twice bigger than that of the other cases.

There are more sums over k for the nonsymmetric QW due to the additional term with coefficient $\Omega_{21}^{(1)}$. In this case the parabolic approximation leads to

$$\xi_\Omega \approx \frac{4\pi e^2 \nu_\Omega |v_{21}|^2}{\sqrt{\epsilon} \hbar c \Omega} n_{2D} \sum_{kk_1\Delta k=-\infty}^{\infty} \frac{J_{k_1}\left(\frac{\Omega_{21}^{(1)}}{\omega}\right) J_{k_1-2\Delta k}\left(\frac{\Omega_{21}^{(1)}}{\omega}\right) J_{k+\Delta k}\left(\frac{\Omega_{21}^{(2)}}{4\omega}\right) J_k\left(\frac{\Omega_{21}^{(2)}}{4\omega}\right)}{[\Omega_{21} - (2k - k_1)\omega - \Omega]^2 + \nu_\Omega^2}. \quad (14)$$

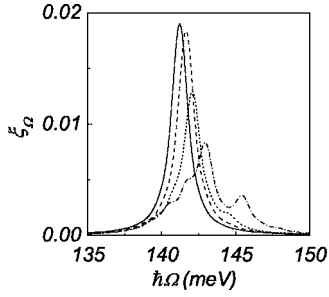


FIG. 4. The relative absorption for nonsymmetric 100 Å QW case under $E_o=10$ kV cm $^{-1}$ and $E_\omega=0$ (solid line), $E_\omega=50$ kV cm $^{-1}$ (dashed line), $E_\omega=70$ (dotted line) and $E_\omega=100$ kV cm $^{-1}$ (dot-dashed line). $\hbar\omega=1.5$ meV and $\hbar\nu=0.66$ meV.

Figure 4 shows the relative absorption of nonsymmetric QW under $E_o=10$ kV cm $^{-1}$ for different E_ω values. In order to obtain a higher relative absorption and a clearer peak structure, we have used parameters corresponding to panel (b) of Fig. 3 ($\hbar\omega=1.5$ meV and $\hbar\nu=0.66$ meV). The behavior of the relative absorption is similar to that of the corresponding to the symmetric case for low fields, but the relative absorption decreases faster and, for fields beyond 70 kV cm $^{-1}$, when the multi-peak fine structure becomes evident, there are clear differences between this case and the symmetric one. Looking at the 100 kV cm $^{-1}$ case in panel (b) of Fig. 3, we can see the symmetry of the relative absorption multi-peak structure with a central maximum and two lateral satellites. On the other hand, Figure 4 shows a clear nonsymmetric fine structure, with a pronounced central maximum located at the same energy than the corresponding to the symmetric case. However, lateral satellites show a strong asymmetry. At first glance it seems that a new plateau appears in the low energy side. Actually, for $E_\omega=100$ kV cm $^{-1}$, both symmetric and nonsymmetric cases present seven relative maxima as can be proven by diminishing the relaxation broadening beyond realistic values. In other words, the absorption multi-peak structure is masked in part by both the THz quanta and the effective relaxation energy values.

IV. NUMERICAL DESCRIPTION

As we have already noted, the perturbation approach is valid under the condition $|e|E_\omega d/2 < \varepsilon_{21}$. If the THz pump is stronger, one needs to perform a numerical solution for the eigenstate problem (3) and to integrate Eqs. (9) and (10) numerically, taking into account the time-dependent velocity matrix element. Such a case can be realized in a wide QW without the requirement of using high fields. Therefore, we will consider below 250 Å wide GaAs-based QWs. In order to check the validity of the parabolic approximation, Fig. 5 shows the relative absorption calculated both by means of this approach and numerically. Calculations are performed for a multiple QW structure with ten decoupled QWs and for a THz quanta energy $\hbar\omega=1.5$ meV. Due to the low values of the energy range in this case (around the optical phonon energy), we consider a step-like function for the relaxation energy taking a smaller value $\hbar\nu=0.5$ meV in the passive

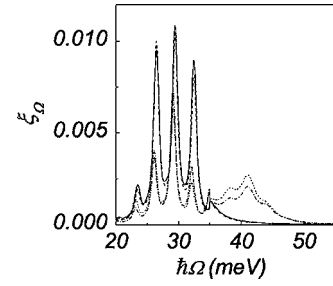


FIG. 5. The relative absorption ξ_Ω obtained through numerical calculations (solid line: $E_\omega=30$ kV cm $^{-1}$, dotted line: $E_\omega=50$ kV cm $^{-1}$) and by means of the parabolic approximation (dashed line: $E_\omega=30$ kV cm $^{-1}$, dash-dotted line: $E_\omega=50$ kV cm $^{-1}$) for the symmetric case and wide QW.

region, when $\hbar\Omega < 35$ meV, and a bigger one $\hbar\nu=1.5$ meV for higher energy values. One can see a very good correspondence between the two methods for fields up to 30 kV cm $^{-1}$ while, for higher fields, the parabolic approach clearly fails.

The results obtained by means of the numerical description for spectral dependencies beyond $E_\omega=30$ kV cm $^{-1}$ are represented in Figs. 6 (symmetric QW) and 7 (nonsymmetric QW). As in Fig. 5, calculations have been made for ten QWs and for the same THz quanta energy and step-like relaxation energy. For higher THz fields the asymmetry appears (even for the symmetric QW). Together with the decreasing and spreading of the relative absorption, the initial peak for $E_\omega=0$ kV cm $^{-1}$ gradually splits in several peaks as the field intensity increases, the number of peaks depending on the intensity. The nonsymmetric QW well case shows two different regions not only due to the stepped relaxation but also because the field runs twice per cycle the region between 0 and E_o-E_ω and only once the remaining region. Thus, the multi-peak fine structure is partially hidden for $\hbar\Omega_{21} > 35$ meV due, once again, to the higher effective relaxation energy.

V. CONCLUSIONS

We have studied the modifications of the intersubband absorption in a multi-QW structure caused by a strong THz irradiation. Experimentally, such an irradiation can be achieved by using free-electron or gas lasers with an energy

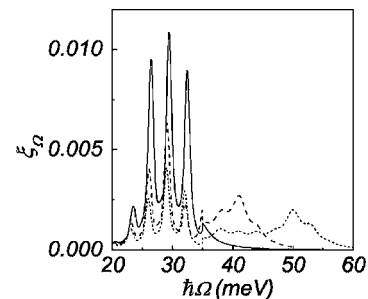


FIG. 6. The symmetric wide QW spectral dependencies of ξ_Ω versus $\hbar\Omega$ for $E_\omega=30$ kV cm $^{-1}$ (solid line), 50 kV cm $^{-1}$ (dashed line), and 70 kV cm $^{-1}$ (dotted line).

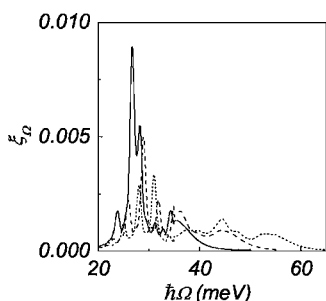


FIG. 7. The nonsymmetric QW spectral dependencies of $\xi_{\beta\Omega}$ versus $\hbar\Omega$ for $E_0=10 \text{ kV cm}^{-1}$ and $E_\omega=30 \text{ kV cm}^{-1}$ (solid line), 50 kV cm^{-1} (dashed line), and 70 kV cm^{-1} (dotted line).

density in the MW cm^{-2} range (see applications of these lasers to study a heterostructure response in Refs. 8 and 9, respectively). Results show a significant fine structure of the absorption peak due to the $(n+1)$ -order intersubband transitions, with n THz photons and a single IR photon. In addition, a strong modification of absorption, which consists on a noticeable broadening of the zero-field peak and a shift towards higher energy values, is also demonstrated. Since the relative absorption calculated is weak enough, one can measure photoconductivity.

We will now discuss the assumptions used in the calculations above. Within the hard-wall scheme we have disre-

garded the underbarrier penetration. In general, for deep and wide decoupled (or weakly coupled) quantum wells, underbarrier penetration slightly modifies wave functions and energy levels position. In the present case and due to the relatively big interlevel distance ($\varepsilon_{21} \sim 140 \text{ meV}$ for narrow QW and $\varepsilon_{21} \sim 30 \text{ meV}$ for wide QW), little changes in the level positions do not affect essential results. For the same reasons we have not taken into account possible contributions of the Coulomb renormalization neglecting the depolarization and exchange effects. We have also used a phenomenological homogeneous broadening energy $\hbar\nu \sim 0.5\text{--}1.5 \text{ meV}$. These assumptions are generally accepted and a possible improvement will not change essentially the obtained results. We have also neglected the interlevel redistribution under THz pump because the interlevel energy ε_{21} is bigger than 20 meV while the THz quanta energy $\hbar\omega$ is around 1 meV . One can neglect a THz field effect on the damping because the influence of such a field on the wave functions is not very strong. Thus, a phenomenological broadening should not be essentially dependent on the THz pump.

To conclude, the present work has shown the possibility that an essential modification of the IR intersubband response takes place when an intense THz irradiation is applied. We expect that the results obtained encourage researchers to carry out experiments in this direction.

*Electronic address: ajhernan@ull.es

¹S. Schmitt-Rink, D. S. Chemla, and D. A. B. Miller, *Adv. Phys.* **38**, 89 (1989).
²H. Haug and S. W. Koch, *Quantum Theory of the Optical and Electronic Properties of Semiconductors* (Word Scientific, Singapore, 1994).
³F. T. Vasko and A. Kuznetsov, *Electronic States and Optical Transitions in Semiconductor Heterostructures* (Springer, New York, 1998).
⁴K. Unterrainer, B. J. Keay, M. C. Wanke, S. J. Allen, D. Leonard, G. Medeiros-Ribeiro, U. Bhattacharya, and M. J. W. Rodwell, *Phys. Rev. Lett.* **76**, 2973 (1996); J. Kono, M. Y. Su, T. Inoshita, T. Noda, M. S. Sherwin, S. J. Allen, and H. Sakaki, *ibid.* **79**, 1758 (1997).
⁵A.-P. Jauho and K. Johnsen, *Phys. Rev. Lett.* **76**, 4576 (1996); K. Johnsen and A.-P. Jauho, *Phys. Rev. B* **57**, 8860 (1998); K. Johnsen and A.-P. Jauho, *Phys. Rev. Lett.* **83**, 1207 (1999).
⁶M. Helm, in *Intersubband Transitions in Quantum Wells: Physics and Device Applications*, *Semicond. Semimetals* 62 1 (2000).
⁷The Bessel-based expansions of the exponential factors used in Sec. III are

$$\exp(iz \cos \psi) = \sum_{l=-\infty}^{\infty} i^l e^{il\psi} J_l(z),$$

$$\exp(iz \sin \psi) = \sum_{l=-\infty}^{\infty} e^{il\psi} J_l(z),$$

$$\exp(z \cos \psi) = \sum_{l=-\infty}^{\infty} e^{il\psi} I_l(z).$$

⁸M. Y. Su, S. G. Carter, M. S. Sherwin, A. Huntington, and L. A. Coldren, *Phys. Rev. B* **67**, 125307 (2003); K. B. Nordstrom, K. Johnsen, S. J. Allen, A.-P. Jauho, B. Birnir, J. Kono, T. Noda, H. Akiyama, and H. Sakaki, *Phys. Rev. Lett.* **81**, 457 (1998).
⁹Z. Y. Lai and W. Z. Shen, *J. Appl. Phys.* **94**, 367 (2003); S. D. Ganichev and W. Prettl, *J. Phys.: Condens. Matter* **15**, R935 (2003).